NOVEL MILES COMPUTATIONS FOR JET FLOWS WITH NOISE

Paul G. Tucker
Fluid Dynamics Research Centre
University of Warwick, Coventry CV4 7AL
P. Tucker@warwick.ac.uk

ABSTRACT

The influence of swirl on jet flow structure and noise is explored. A novel DES (Detached Eddy Simulation) type procedure is tested for a jet with co-flow case. The approach uses a *k-l* near wall RANS (Reynolds Averaged Navier-Stokes) model. Away from walls MILES (Monotone-Integrated Large Eddy Simulation) is used. Blending of the RANS and MILES regions is achieved using a Hamilton-Jacobi type equation. The MILES solution content enables correct turbulence evolution on relatively coarse grids. The new DES/MILES (*DESmiles*) approach is validated for a plane channel flow. A good law of the wall is gained. For swirling flows, far-field noise levels are calculated using the surface integral of Ffowcs Williams and Hawkings. Despite MILES use with mostly 4^{th} order centered differencing, turbulence decays excessively downstream. Streamwise vorticity introduced by swirl (unlike with chevrons) increases noise. Lower swirl levels might bring more success. *DESmiles* appears promising. However, for the jet with co-flow case (due to the low co-flow Reynolds number) it is perhaps only mildly tested.

INTRODUCTION

The accurate prediction of jet flows is important for the reduction of jet engine noise and combustion system performance. Swirling flows have been considered in the context of increased combustion mixing and noise reduction (see Mehta et al., 1991). Often, in aero engines a primary jet is surrounded by a slower moving co-flow giving a velocity difference ΔU. Evidence suggests (see Morse, 1980) that the initial interaction of the co-flow with the primary has a strong flow structure influence. The work of Papamoschou and Debiasi (2001) indicates that the interaction between the co and core flow also has a profound sound level influence. Various novel devices have recently been considered to reduce jet noise by breaking down larger more coherent turbulence structures through the generation of smaller structures. A key example is the use of serrated nozzles (chevrons). These introduce streamwise vorticity. The numerical study of the delicate turbulence interactions required to reduce noise is perhaps best carried out through LES (Large Eddy Simulation) related techniques. These are generally not, as with RANS, so dependent on calibration for different flow types. Shur et al. (2002) make MILES jet noise predictions. The grid is fine enough to resolve shear layer roll-up. However, a key observation from this work is that use of Smagorinsky type subgrid scale (sgs) LES models results in excessive turbulence transition delay. The subgrid models do not have the physics to adequately model the strongly sheared mixing layer region (Kosovic,

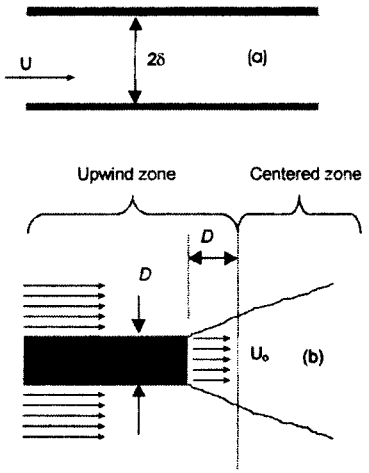

Figure 1. Geometries considered: (a) plane channel and (b) jet with co-flow.

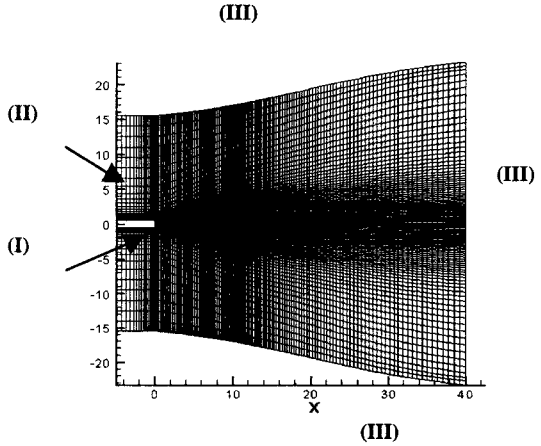

Figure 2. *x-y* plane solution grid.

1997). Also, in the work of Shur et al., turbulence intensities tend to be under-predicted. This observation also seems to add strength to MILES use. The work of Shur et al. is extended here in the following two ways: (a) the influence of swirl on flow structure and noise level is explored and (b) a novel zonal LES procedure is tested for a jet with co-flow case.

As in the work of Tucker and Davidson (2003), the novel zonal LES approach uses a *k-l* near wall RANS model. Away from walls MILES is used (the hybrid DES like approach is referred to here as *DESmiles*). In this way the LES delayed turbulence transition observed by Shur et al. is avoided. The near wall RANS length scale evaluation involves Eikonal (Sethian, 1999) equation use. Blending of the RANS and MILES regions is achieved by the addition of a Laplacian scaled by normal wall distance (*d*) to the Eikonal equation. The blending is important. Any discontinuities are likely to introduce spurious noise modes. The new approach is initially tested for the Figure 1a plane channel flow. For the swirling flows, far-field jet noise level computations are made. For these predicted acoustic fluctuations are fed into a simplified version of

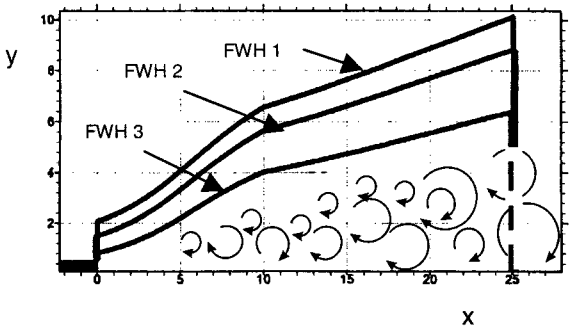

Figure 3. Locations of FWH.

the surface integral equation of Ffowcs Williams and Hawkings (1969) (FWH). Sound level comparisons are made with the non-swirling flow measurements of Lush (1971) and Tanna (1977). In this way the sound influence of swirl can be better discerned.

NUMERICAL METHOD

Governing equations.

To capture acoustic waves, as observed by Shur et al., the equations should be solved in their compressible form. Conservation of momentum can be expressed using Equation (1) below:

$$\frac{\partial \rho \tilde{u}_i}{\partial t}+\frac{\partial \rho \tilde{u}_i \tilde{u}_j}{\partial x_j}=-\frac{\partial \tilde{p}}{\partial x_i}+\frac{\partial}{\partial x_j}\left[(\mu+\mu_T)\left(\frac{\partial \tilde{u}_i}{\partial x_j}\right)\right] \quad (1)$$

The symbol $\tilde{u}_i$ is a fluid velocity component, ρ density, μ viscosity, $\tilde{p}$ static pressure, t time and x the spatial co-ordinate. The tilde is used to identify that near walls

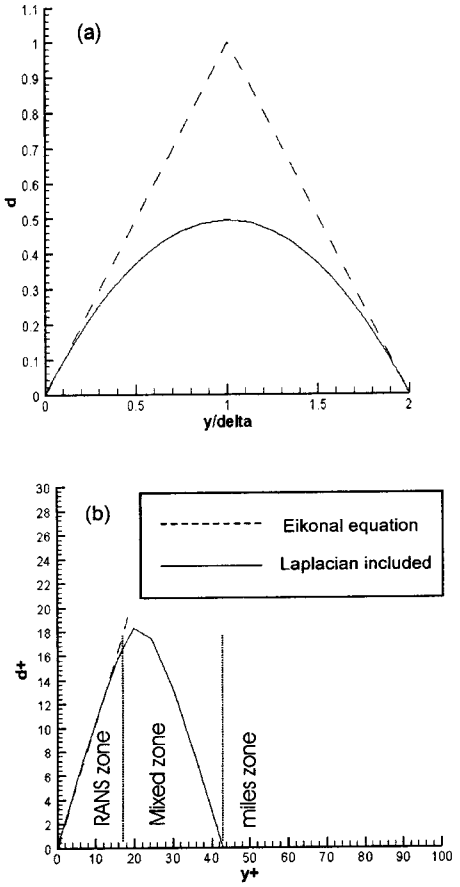

Figure 4. Eikonal based distances for plane channel flow: (a) RANS scales and (b) DESmiles

traditional RANS time averaging is applied and that elsewhere MILES is implemented. Consequently, in the RANS region $\mu_T = \mu_t$, the eddy viscosity. In the MILES zone $\mu_T = \mu_{sgs} = 0$ i.e. effectively $\mu_T = \mu_{num}$ the numerical diffusion. The continuity equation corresponding to the above is

$$\frac{\partial \rho}{\partial t}+\frac{\partial \rho \tilde{u}_j}{\partial x_j}=0 \quad (2)$$

Zonal turbulence model details

The modelled turbulent kinetic energy, *k*, equation is as follows:

$$\frac{\partial \rho k_T}{\partial t}+\frac{\partial \rho \tilde{u}_i k_T}{\partial x_i}=\frac{\partial}{\partial x_j}\left[(\mu+\frac{\mu_T}{\sigma_k})\left(\frac{\partial k_T}{\partial x_j}\right)\right]$$

$$+P_{k_T}-\frac{\rho k_T^{3/2}}{l_\varepsilon} \quad (3)$$

where P_{k_T} is the turbulence production term. Again the 'T' subscript is used to differentiate between MILES and RANS related components. For the MILES zone $k_T = k_{sgs} = 0$. For the RANS region, the k-l model of Wolfshtein (1969) is used where $\mu_T = \rho C_\mu l_\mu k_T^{1/2}$, $l_\varepsilon = C_l d(1-e^{-A_\varepsilon y^*})$, $l_\mu = C_l d(1-e^{-A_\mu y^*})$ and $y^* = d\rho k^{1/2} C_\mu^{1/4}/\mu$. Constants have the following values:

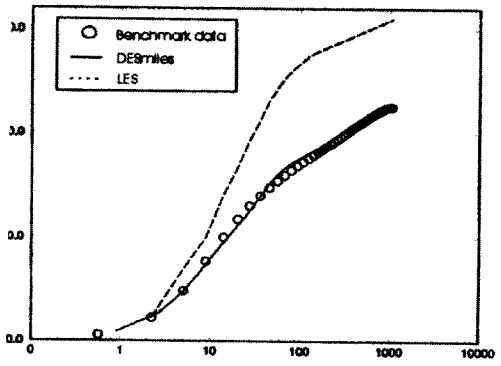

Figure 5. DESmiles law of the wall for plane channel flow

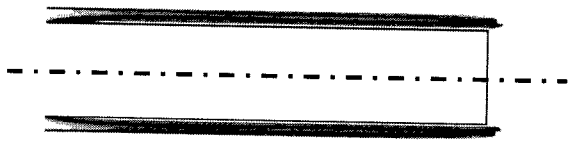

Figure 6. Modelled k contours for jet with co-flow

C_μ=0.09, C_l=2.4, A_μ=0.016, A_ε=0.263 and σ_k=1. The distance d is evaluated from a Hamilton-Jacobi (HJ) equation (Tucker, 2003)

$$|\nabla d| = 1 + f(d)\nabla^2 d + g(d) \qquad (4)$$

Here $f(d) = \varepsilon_0 d$ and $g(d) = \varepsilon_1 (d^e/L)^n$. The length scale L is the RANS region width and n a positive integer. When $\varepsilon_0 = \varepsilon_1 = 0$, Equation (4) reduces to the hyperbolic natured Eikonal equation. This gives exact wall distances $d^e = d$. The Eikonal equation can be solved by propagating fronts from solid surfaces (Sethain, 1999). Here, the equation is propagated towards the RANS/miles interface. Then at the interface, the condition $d=0$ is set and the equation solved with ε_0, $\varepsilon_1 > 0$. The Laplacian enables a smooth transition between the modelled RANS length scale and the MILES zone. The function $g(d)$ can be used to control the RANS length scale in the vicinity of the miles zone (see later). Despite the simple appearance of the Eikonal and Equation (4), they are not trivial to solve (see Tucker, 2003).

Solution of flow governing equations

The flow governing equations are solved using a modified version of the NTS code of Shur et al. (2002). The problem set-up is virtually identical to that in the paper of Shur et al. Therefore, only brief details are given here. An x-y plane view of the solution grid is shown in Figure 2. The grid comprises two blocks. The much smaller inner 'axis' block has a radial extent of approximately 0.2. It is intended to avoid an axis singularity. Since, none of this block's faces are wall adjacent, when solving (4) it is ignored. The total number of grid points is 500,000. At the Figure 2 boundaries, labelled **(III)**, sponges, are applied in the manner of Ashcroft and Zhang (2001). Flow boundaries **(I)** and **(II)** use Dirichlet conditions. Simulated flow inlet turbulence levels are zero. A hybrid convective flux differencing discretization is used. The furthest right Figure 1b dashed vertical line, at $X=D$, essentially indicates where the convective differencing changes. To the right of this line nearly 4th order centered differencing is used. To the left, encompassing the miles zone, 5th order upwind is used. The two are blended using the following equation $J_{conv} = (1-\alpha)J_{ctr} + \alpha J_{upw}$ where J_{ctr} and J_{upw} are the centered and upwind flux components and α is the blending function. The latter varies smoothly between $X=0$ and $X=D$. The smallest usable value of α is 0.25. A second-order, 3-layer time integration is used with a time step $\Delta t = 0.04 D/U_o$. Simulations need $t \cong 2000 D/U_o$.

Noise postprocessor

The NTS acoustic postprocessor yields far-field acoustic pressure fluctuation approximations p'. This is achieved by application of the following simplified (the quadrupole volume integral related source term is omitted) FWH surface integral theory

$$4\pi|\mathbf{x}|p'(\mathbf{x},t) = \frac{x_j}{|\mathbf{x}|a}\frac{\partial}{\partial t}\left[\int_S \{p' n_j + \rho u_j u_n\} dS\right] + \frac{\partial}{\partial t}\left[\int_S \{\rho u_n\} dS\right] \qquad (5)$$

The Equation (5) solution around the three Fig. 3 (FWH 1, FWH 2 and FWH 3) surfaces (S) is considered. These are located where there are no turbulence fluctuations i.e. it is attempted to position the surfaces where fluctuations are purely acoustic and hence the flow irrotational. For this reason, none of the surfaces are closed at X = 25. The lack of closure is a key area of modelling uncertainty (see Shur et al. (2002)). For jets with co-flow, core flow turbulent eddies will be drawn down stream even further. This will worsen the modelling uncertainty. In the above, u_j are velocity components, u_n is the surface normal velocity component, $\mathbf{x}$ the observer position and a the speed of sound.

DISCUSSION OF RESULTS

Wall distance and DESmiles approach

Initially, it is helpful to consider Eikonal and HJ wall distance equation traits. Tucker (2003) gives extensive further examples for various geometries. Here, examples are first considered for the Figure 1a plane channel. This is infinite in x and y. Figure 4 gives Eikonal/HJ based distances. Frame (a) gives RANS suitable distances and (b) *DESmiles*. The full and dashed lines are Equation (4) $\varepsilon_1 = 0$ solutions with $\varepsilon_0 \neq 0$ (HJ) and $\varepsilon_0 = 0$, respectively. To make the Frame (a) Laplacian smoothing influence clear $\varepsilon_0 = 2$ i.e. a large value. The resulting reduced d scale means the turbulence damping influence of both walls is now correctly sensed (Fares and Schroder, 2002). Frame (b) illustrates the beneficial *DESmiles* Laplacian smoothing effect. For this, the pure MILES zone is set at $y^+ \approx 43$. The maximum-modelled length scale will be centered between the wall and MILES zone, at $y^+ \approx 21.5$. To bias the peak towards to MILES zone $\varepsilon_1 > 0$ can be used.

It might seem most sensible to have the RANS zone extend beyond the buffer layer and well into the inner logarithmic region, without any diminishment of the modelled turbulence. However, experience suggests (Temmerman et al., 2002) that better results are gained if the RANS region influence is diminished. This is because MILES zone activity will force resolved scales in the RANS regions. The sum of these resolved and modelled scales will yield excessive turbulence energy. Figure 5 gives the Re_τ = 1050 law of the wall for the current approach. The symbols are the benchmark LES data of Piomelli (1993). The full and dashed lines represent *DESmiles* and LES predictions, respectively. There has been absolutely no *DESmiles* parameter tuning. The MILES location is set at $y^+ \approx 43$ with $\varepsilon_0 = 0.2$, $\varepsilon_1 = 0$ and the reasonable Figure 5 law of the wall found. Normal stress turbulence statistics also show pleasing agreement with benchmark data. Clearly for the coarse grid the LES is poor. Reflecting HJ computed distances, Figure 6 gives modelled k contours for a co-flowing jet *DESmiles*. For the jet Re=1x10^4 and ΔU = 0.27. The MILES location and ε values are chosen to match those used for the plane channel.

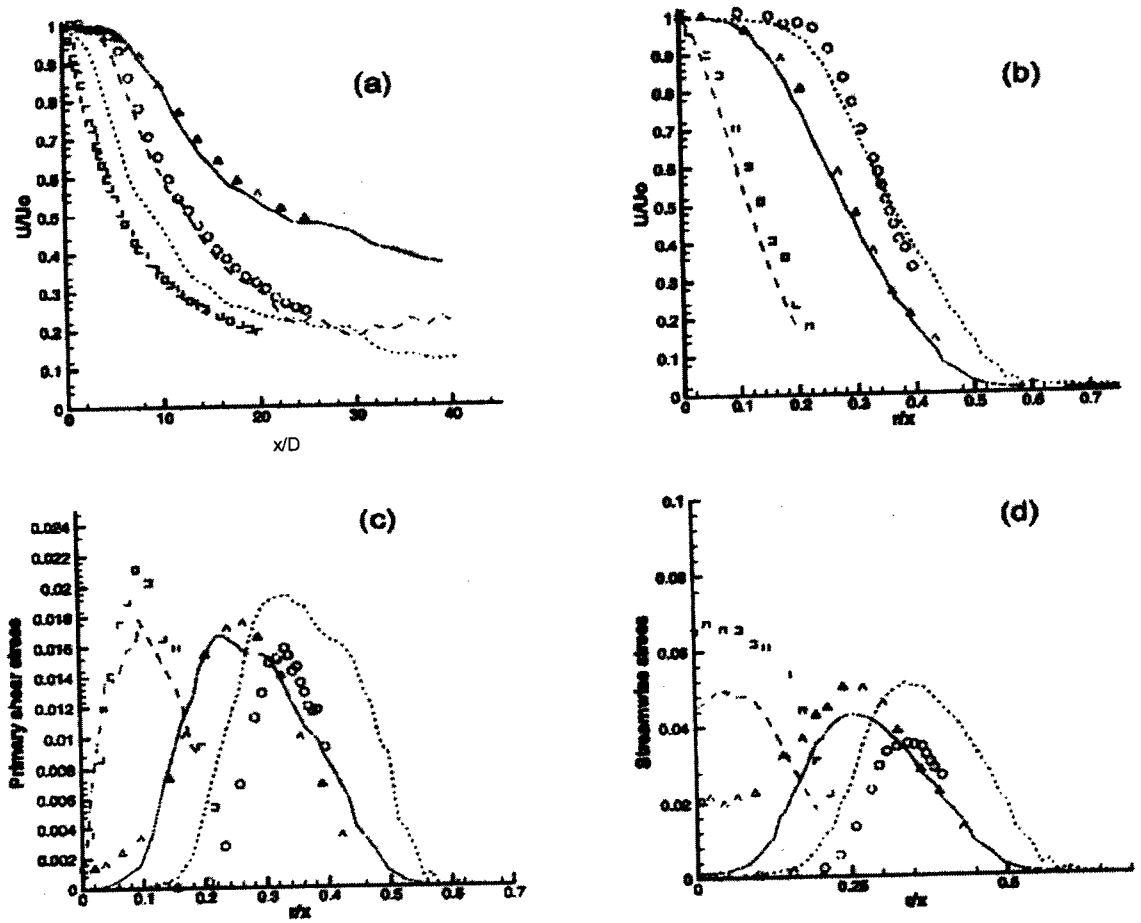

Figure 7. Jet mean velocity and turbulence statistics profiles for: (a) axial velocity centre line decay; (b) radial variation of axial velocity; (c) radial variation of shear stress and radial variation of normal stress.

Jet flow cases

Four mostly aero acoustic motivated jet cases are now considered. These are: (i) a plane jet with no swirl (i.e. S = 0), (ii) case (i) with a uniform swirl profile giving $S \approx$ 0.225 (the swirl number is conventionally defined); (iii) case (ii) but with the swirl velocity (w) heavily concentrated towards the inlet outer radius such that $w = C_0 U C_1^r r^n \cos(\pi r)$ where C_o=54x10^4, C_1=2.7182818, (iv) case (i) with co-flow (ΔU=0.27). When $\Delta U > 0$, the co-flow velocity and hence turbulence levels are low (0.3%). Therefore, near wall modelling is not strongly tested. However, according to Morse (1980) the co-flow nature at the jet exit exerts a key influence and so it seems important to correctly model the co-flow boundary layer.

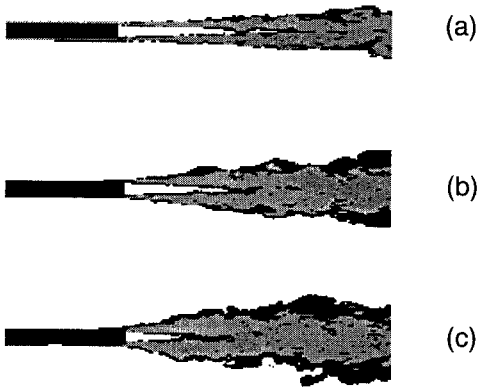

Figure 8. Instantaneous vorticity plots: (a) swirl; (b) no-swirl and (c) co-flow.

Figure 7 compares jet mean velocity and turbulence statistic profiles with measurements. The measurements of Morse (1980) and Mehta (1991) are for S = 0.2 and 0.25. Consequently, for the predictions $S \approx$ 0.225. Frame (a) compares (normalised by jet outlet velocity U_o) centre line velocity decay predictions with Morse's measurements. Moving left to right, the three comparison sets correspond to ΔU=0 with a $S \approx$ 0.225 (short dashed line with squares), $\Delta U = S = 0$ (long dashed line with circles), and ΔU = 0.27, S=0 (full line with triangles). Clearly, $S > 0$ reduces the jet potential core region and co-flow extends it. The larger $S >$ 0 discrepancy is partly attributed to the fact that the swirl in the experiment would tend to stagnate the jet axis region flow. The predictions, however, use $u \neq f(r)$. Also, for $S > 0$, there are sharper velocity gradients. This will place stronger grid demands. Therefore, for this more challenging turbulence physics case a lower level of agreement is perhaps to be expected.

Frames (b), (c), and (d) compare, $S > 0$, $\Delta U = 0$ predictions with measurements for the radial variation of normalised mean axial velocity, normal ($\overline{u'u'}/U_o^2$) stress and shear ($\overline{u'v'}/U_o^2$) stress, respectively. Comparisons are made at x/D = 1.5, 2 and 10. The circle, triangle and square symbols are with increasing x/D. The more modern x/D = 1.5 measurements are due to Mehta. Overall the agreement is encouraging. However, the tendency for stress over-prediction adjacent to the jet outlet and under prediction away from it are clear. A finer grid should improve this trait. The excessive drop of predicted turbulence intensities with increasing x/D justifies the proposed reduced dissipation *DESmiles* approach.

Figure 8 gives x-y plane vorticity contours for flows (iv), (i) and (ii), respectively. The presentation order is based on the increasing potential core length observation (see Figure 7a). The increasing jet spreading rate for $S > 0$ is evident. Figure 9 gives predicted r-z plane acoustic range pressure (p) contours for ΔU=0, S>0 and the swirl heavily concentrated towards the jet outer radius. The p contours appear very similar to those for S=0 (not shown). The acoustic range p contours for ΔU>0 (not shown here) suggests the co-flow has a significant acoustic wave blocking influence. The Figure 10 lower frames give predicted r-θ plane streaklines and p contours at x/D = 0.5 for flows (iii) - $S \approx$ 0.225, ΔU=0 -, (i) - S = 0, ΔU=0 -, and (iv) - S =0 , ΔU = 0.27, respectively. The top row shows

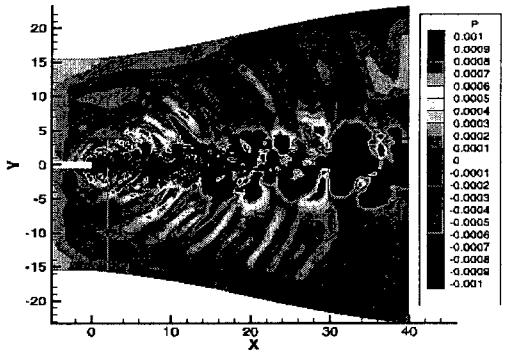

Figure 9. Acoustic range pressure contours.

flow visualisation results by Ng (2000) for an 8 lobed nozzle. The frame (a) $S \approx$ 0.225 simulation shows clockwise streamwise vorticity regions at the jet edge. These have the potential to break up larger coherent structures and influence sound levels. The streamwise vorticity is also evident in the results of Ng. The non-lobed predictions look similar to the lobed observations of Ng. Frame (b) with S=ΔU=0 again seems similar the Ng visualisation having contra-rotating vortex pairs. Predictions suggest that the lobes of Ng might not necessarily be the full flow structure controlling factor - the general flow features observed by Ng are also present in the simulations. Frame (c) suggests that co-flow substantially reduces streamwise vorticity.

Figure 11 compares predicted far-field sound levels for S = 0.225 with the S = 0 measurements of Lush (1971) and Tanna (1977). Results are shown for FWH surfaces 1-3. Some sensitivity to the FWH surface configuration can be observed. Predictions for S=0 (see Shur et al. (2002)) are in agreement with the measurements. Therefore, the present swirl level has produced more noise. However, the successful chevron approach also initially produced more noise. Careful tuning with respect to swirl profile and level could be required to ensure the added turbulence correctly modifies larger coherent structures.

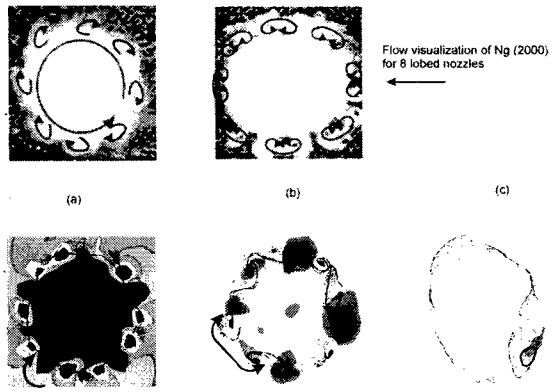

Figure 10. Flow structure at $x/D = 0.5$ in r-θ plane: (a) swirl; (b) no-swirl and (c) co-flow.

The work of Papamoschou and Debiasi (2001) suggests that when $\Delta U \neq 0$, reduction of the potential core extent gives noise reductions. This is because the end of potential core region is a major noise source. Shortening this region maximises the co-flows sound shielding potential. As the results here show, swirl has the desirable property of shortening the potential core region. Therefore, exploring the effect of swirl when there is co-flow seems worthwhile and will hopefully be the subject of future work. However, the $\Delta U \neq 0$ FWH surface integral implementation would need consideration.

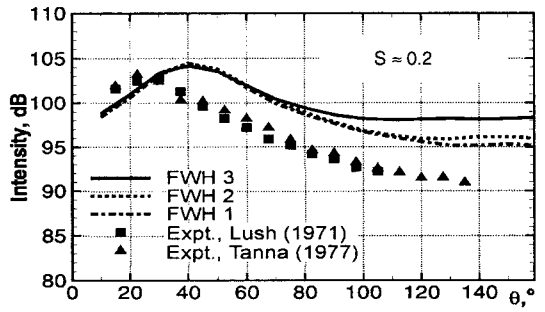

Figure 11. Comparison of predicted and measured far field noise

CONCLUSIONS

The influence of swirl on flow structure and jet noise was explored. The jet Reynolds number was 1×10^4. The novel *DESmiles* procedure was tested for a plane channel and jet with co-flow. Blended RANS/MILES region implied turbulence length scales were computed using a Hamilton-Jacobi equation. The blending is important. Discontinuities are likely to introduce spurious noise modes. For the channel, a good law of the wall was gained with no parameter tuning. Despite the use of MILES, 500,000 cells and mostly 4th order centered differencing, jet turbulence still has excessive downstream decay. The streamwise vorticity introduced by swirl increased noise. Further swirl profile/level optimisation work might be worthwhile along with co-flow studies. *DESmiles* appears promising. However, for the jet with co-flow case it was only very mildly tested.

ACKNOWLEDGEMENTS

I would like to thank P. Spalart, M. Shur and M. Strelets for their kind help and the use of their excellent code.

REFERENCES

Ashcroft, G., and Zhang, X., 2001, "A computational investigation of the noise radiated by flow induced cavity oscillations," *AIAA Paper*, AIAA 2001-0512.

Fares, E., and Schroder, W., 2002, "A differential equation to determine the wall distance," *Int. J. for Num. Meths in Fluids*, Vol. 39, pp 743-762.

Ffowcs Williams, J. E., and Hawkings, D. L., 1969, "Sound generation by turbulence and surfaces in arbitrary motion," *Phil. Trans, Royal Society of London*, Series A, Vol. 264, May 8, pp. 321-342.

Kosovic, B., 1997, "Subgrid scale modelling for the large eddy simulation of high Reynolds number boundary layers," *J. Fluid Mech.*, Vol. 336, pp. 151-182.

Lush, P. A., 1971, "Measurements of subsonic jet noise and comparison with theory," *J. Fluid Mech.*, Vol. 46, Pt. 3, pp. 477-500.

Mehta, R. D., Wood, D. H, and Clausen, P. D., 1991, "Some effects of swirl on turbulent mixing layer development," *Phys Fluids*, A3, Vol. 11, November.

Morse, A. P., 1980, "Axisymmetric turbulent shear flows with and without swirl," *PhD Thesis University of London.*

Ng, T. T., 2000, "Visualisation study of a passively perturbed swirling jet," *AIAA J.*, Vol. 39, No. 1: Technical Notes, pp. 188-190.

Papamoschou, D., and Debiasi, M, 2001, "Directional suppression of noise from a high-speed jet," *AIAA J.*, Vol. 39, No. 3, pp. 380-387, March.

Piomelli, U., 1993, "High Reynolds number calculations using the dynamic subgrid-scale stress model," *Phys. Fluids*, Vol. 5, pp. 1484-1490.

Sethian, J.A., 1999, "Fast Marching Methods," *SIAM Review*, Vol. 41, No. 2, pp. 199-235.

Shur, M. L., Spalart, P. R., Strelets, M. Kh, and Travin A. K., 2002, "Towards the prediction of noise from jet engines," *Proc. 5th Int. Symp and Engineering Turbulence Modelling and Measurement*, Mallorca, Spain, 16-18 September, pp. 699-708.

Tanna, H. K., 1977, "An experimental study of jet noise," Part I: Turbulent Mixing Noise, *J. Sound and Vibration*, Vol. 50, No. 3, pp. 405-428.

Temmerman, L., Leschziner M. A., and Hanjalic, K., 2002, "A-priori studies of a near-wall RANS model within a hybrid LES/RANS scheme," *Engineering Turbulence Modelling and Experiments* – 5 (Eds. W. Rodi and N. Fueyo), Elsevier Science, pp. 317-326.

Tucker, P. G., and Davidson, L., 2003, " Zonal k-l based large eddy simulations," *AIAA Paper*-2003-0082.

Tucker, P. G., 2003, "Differential equation based length scale evaluations for DES, RANS and moving grid solutions," *Proc. 3rd Int. Symp. on Turbulence and Shear Flow Phenomena*, TSFP3, Sendai, Japan, June 25-27.

Wolfshtein, M., 1969, "The velocity and temperature distribution in one-dimensional flow with turbulence augmentation and pressure gradient," *Int. J. Heat and Mass Transfer*, Vol. 12, pp. 301-318.